ADVANCED FUNCTIONAL MATERIALS
www.afm-journal.de

Enhanced Photocatalytic Activity of Au/TiO_2 Nanocomposite Prepared Using Bifunctional Bridging Linker

*Marko Miljevic, Bianca Geiseler, Thomas Bergfeldt, Pascal Bockstaller, and Ljiljana Fruk**

Using a simple bifunctional bridging linker, nanosized gold and titanium dioxide composites are prepared containing different Au loadings. Linker is synthesized to contain both catechol and thiol moieties to enable binding to the TiO_2 and Au surface respectively. Au/TiO_2 nanocomposites are prepared using simple synthetic route that allows the control over the amount of Au nanoparticles, a property which plays a significant role in the catalytic activity of hybrid materials. Photocatalytic activity of materials prepared using different TiO_2 precursors is investigated using reactive oxygen species sensitive assay based on activation of horseradish peroxidase (HRP) enzyme. Significant increase in catalytic activity is observed for all Au/TiO_2 nanocomposites with Au/TiO_2 prepared by use of the bridging linker being up to 5.5 times more active than bare commercial TiO_2 nanoparticles. In addition to 365 nm light excitation, less energetic 470 nm light, which is more suitable for the use with biological systems, is used to induce photocatalytic activity. Finally, prepared photocatalytic materials are successfully used to exert temporal control over enzymatic activity, a feature which is important for the study of both enzymatic activity and design of novel bio-sensing platforms.

1. Introduction

TiO_2 is a large electron gap semiconductor with good chemical and thermal stability and excellent electronic and optical properties, due to which it has found numerous applications in the field of photo-catalysis and dye sensitized solar cells.[1] Nanostructured TiO_2 semiconductors are also extensively explored for solar energy triggered fuel production through, for example, water splitting, which further increased the interest in understanding the behavior of interfacial electron and hole transfer.[2] Namely, it has been shown that depending on the size and the surface modification, TiO_2 nanostructures can be photo-activated by UV or visible light to induce the generation of electron–hole (e-/h+) pairs, which can be exploited for various processes at the TiO_2 interface.[3] Particularly interesting is the ability of generated electron–hole pairs to recombine with water and oxygen molecules in the proximity of the TiO_2 surface leading to the production of reactive oxygen species (ROS). For example, when TiO_2 NPs are irradiated with UV light, the surface bound hydroxyl groups can scavenge the photogenerated holes to produce hydroxyl radicals and this ability was exploited in a number of applications ranging from photocatalytic degradation of pollutants,[4] oxidation catalysis in organic chemistry,[5] enzyme activation, and even designing coatings for smart textiles, in which stains and odors can be removed by exposure to solar light.[6]

One of the significant factors, besides size and shape,[7] which influences photocatalytic performance of TiO_2 NPs is their crystal form. Li and colleagues have shown, using H_2 evolution as an indicator, that pure rutile phase shows very poor photocatalytic activity when compared to more superior anatase or anatase-rutile NPs phase junction.[8] In the last decade, a number of studies have shown that noble metal NPs enable size dependent storage of electrons, which can then be released to the suitable acceptors.[9] When coupled to semiconducting materials such as TiO_2, noble metal NPs can facilitate the shuttling of the photoexcited conduction band electrons to the species in the solution and so improve the photocatalytic performance as the charge carriers escape the recombination and can be involved in other processes at the nanomaterial interface.[10] Recently, it has been reported that electron transfer from gold (Au) NPs to TiO_2 occurred under irradiation of visible light due to surface plasmon resonance (SPR).[9c,11] Au NPs have been particularly interesting in nanocomposite preparation for photocatalysis due to their stability, ease of preparation, and remarkable electronic and optical properties. Valden et al. investigated the particle size effect on the catalytic activity of Au dispersed TiO_2 surface and found out that the maximum

M. Miljevic, B. Geiseler, Dr. L. Fruk
Karlsruhe Institute of Technology
DFG-Center for Functional Nanostructures
Wolfgang-Gaede-Str.1a, 76131, Karlsruhe, Germany
E-mail: ljiljana.fruk@kit.edu
Dr. T. Bergfeldt
Karlsruhe Institute of Technology
Institut für Angewandte Materialien Angewandte Werkstoffphysik (IAM-AWP)
Hermann-von-Helmholtz-Platz 1, 76344 Eggenstein-Leopoldshafen
Karlsruhe, Germany
P. Bockstaller
Karlsruhe Institute of Technology
Laboratory for Electron Microscopy (LEM)
Engesserstr. 7, 76131, Karlsruhe, Germany

DOI: 10.1002/adfm.201301484

activity enhancement was achieved for Au NPs around 5 nm or smaller, which was later confirmed by other researchers.[12a] Kowalska et al. reported that particle sizes of both TiO_2 and Au are the key factors for high level of activity.[13] In most studies on Au/TiO_2 nanocomposites, photogenerated TiO_2 electrons were used to reduce the Au precursor to afford photodeposition of Au NPs onto TiO_2 support, which complicates the preparation process and often leads to the lack of control over the size distribution. Recently, Tanaka et al. successfully loaded colloidal gold nanoparticles onto TiO_2 using a method of colloid photodeposition in the presence of hole scavenger (CPH), and have shown that the catalytic activity in the mineralization of organic acids under visible light was highest at 1 wt% Au.[14]

Seh et al. developed a method for anisotropic growth of TiO_2 onto spherical and rod shaped Au NPs using hydroxyl-propyl cellulose as a stabilizing agent and showed that the catalytic activity towards reduction of 4-nitrophenol is significantly enhanced.[15] Liang and colleagues used green chemistry methodologies to prepare Au nanoparticles, which were then deposited onto commercial TiO_2 and tested for oxidative decomposition of Orange G showing enhancement of catalytic performance compared to the TiO_2 alone. In the presented study we have examined the use of rationally designed bridging linker to enable controlled attachment of Au onto TiO_2 NP or in situ synthesis of Au/TiO_2 nanocomposite. Further on, we have demonstrated that such a simple synthetic rout allows a production of Au/TiO_2 hybrids with well controlled Au loadings. As we are particularly interested in use of this material for bio-activation, we studied the catalytic properties employing the ROS production and enzyme activation to assess the activity enhancement both under UV and visible light irradiation. Moreover, we have shown that the use of Au/TiO_2 can enable temporal control over the enzymatic activation under visible light, which could lead to the development of novel bio-catalytic platforms.

2. Results and Discussion

2.1. Preparation of Au/TiO_2 Hybrid Materials Using Bifunctional Linker

Recently reported methodologies to prepare hybrid Au/TiO_2 materials rely on the deposition of Au NPs or Au, for example, through vapor or photo-deposition onto commercial TiO_2. [14,16] To improve the metal nanoparticle-TiO_2 interaction, which might also effect the interfacial charge transfer processes and exert a certain control over the synthetic procedure,[17] we have prepared a bifunctional linker (N-(3,4-dihydroxyphenethyl)-5-(1,2-dithiolan-3-yl)pentanamide) (LA-DA) **1** (**Figure 1**) containing the catechol moiety for TiO_2 attachment and thiols as strong Au binding functional groups. Such linker acts as an effective bridge between two materials enabling the preparation of novel hybrids using different strategies that might affect their photocatalytic properties. In order to

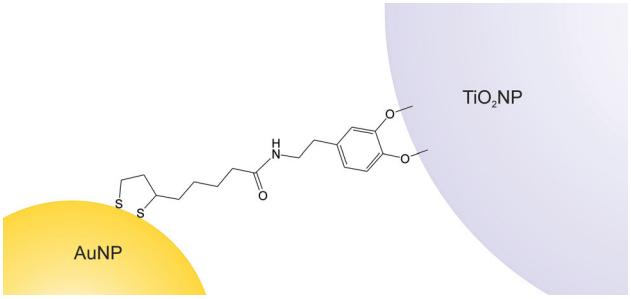

Figure 1. The scheme of the Au NP – TiO_2 NP interaction using lipoic acid–dopamine bridging linker-**1**.

obtain Au/TiO_2 hybrid structures, AuNP-**1** (< 5 nm) were synthesized using optimized one pot $NaBH_4$ gold salt reduction procedure in presence of the bridging linker and characterized by transmission electron microscopy (TEM) and zeta-potential measurements, which confirmed strong stabilizing effect of the linker with zeta-potential measuring –43 mV (Supporting Information, Figure S1a–c). It was shown previously that the photocatalytic properties of hybrid materials decrease significantly upon increase of the Au NP size and NP of around 4 nm have been indicated as to be amongst the most effective ones.[10c,18] Two approaches were employed to obtain Au/TiO_2 for further exploration of different factors that might affect the photocatalytic activity. The first approach involved binding of AuNP-**1** and commercially available TiO_2 NPs to obtain Au-**1**/TiO_2A (**Figure 2**a) and second one utilized the AuNP-**1** as seeds for TiO_2 growth using TiF_4 as precursor resulting in Au-**1**/TiO_2B (Figure **2**b). It should be noted that, to date, many different TiO_2 precursors have been used for preparation of crystalline nanostructures; among them are $TiCl_4$,[19] titanium tetraisopropoxide (TTIP),[15a,20] tetrabutyl titanate (TBOT), or titanium tetrabutoxide (TTB).[21] We have used TiF_4 as it has a lower hydrolysis rate and therefore enables slower and gradual

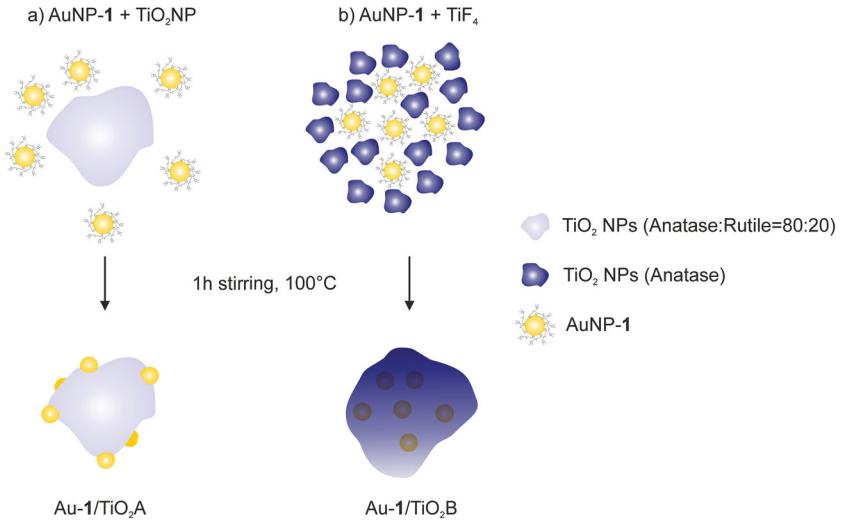

Figure 2. Two synthetic routes used for the preparation of Au/TiO_2 nanocomposites a) binding of AuNP-**1** to TiO_2 NPs to obtain Au-**1**/TiO_2A and b) use of AuNP-**1** as seeds to prepare Au-**1**/TiO_2B.

Table 1. Au/TiO_2 nanocomposites used in this study.

Hybrid Name	AuNP stabilizer	TiO_2 precursor
Au-**1**/TiO_2A	Linker-**1** (LA-DA)	Commercial TiO_2NP
Au-**1**/TiO_2B	Linker-**1** (LA-DA)	TiF_4
Au-**2**/TiO_2A	Linker-**2** (Citrate)	Commercial TiO_2NP
Au-**2**/TiO_2B	Linker-**2** (Citrate)	TiF_4

growth of TiO_2 shells as shown by Wang et al. in their work on TiO_2 nanocage synthesis.[18a] In addition, to investigate the role of linker-**1**, citrate coated AuNP-**2** (Supporting Information, Figures S2a–c) were utilized as Au precursor for preparation of control hybrid materials (Au-**2**/TiO_2 A and Au-**2**/TiO_2B). Such synthetic protocol resulted in four distinct types of nanocomposite based on the use of two different bridging compounds, linker-**1** (LA-DA) and linker-**2** (Citrate) (**Table 1**). From the vast body of literature, it is still not really clear which Au loading should be used in Au/TiO_2 hybrid synthesis to obtain hybrid material with superior photocatalytic properties. Almost two decades ago, Bamwenda et al. have shown that the photo-catalytic properties of Au/TiO_2 hybrids vary significantly with Au to TiO_2 ratio, with highest activity reported for approximately 1 wt% of Au.[22] Since then, and in contrast to the previously referred work, other groups have claimed that both higher and lower Au percentages result in higher photocatalytic activity of the hybrids.[23] To explore the effect of Au wt%, we have prepared hybrids with an extensive range of Au loadings (0.1–50 wt%), which resulted in the significant difference in the color of the suspensions (**Figures 3**a,b). Subsequent TEM analysis indicated corresponding differences in the amount of Au present in the hybrid (**Figure 4**a,b), while the confirmation of the exact Au loadings came from the inductively-coupled plasma mass spectrometry (ICP-MS) measurements that are given in the **Table 2**. These results clearly show that we have developed a very simple synthetic route to accurately control the loading of AuNPs onto the surface of commercially available TiO_2 NPs in a very wide range (0.1–50% Au loading). Slightly bigger disagreement between the theoretically calculated Au loadings and those measured by ICP-MS in case of Au-**1**/TiO_2B hybrids, can be explained by the experimental setup in which slow hydrolysis of TiF_4 precursor is the limiting factor where optimization of the reaction time could lead to even more precise ratios. However, it should be emphasized that the described methodology of hybrid synthesis allows the adjustment of the Au loading while keeping the same size distribution of Au NPs. This, in turn, enables us to investigate only the influence of the Au loading on photocatalytic properties of the hybrids as the size is controlled. Other methods used in hybrid synthesis often do not allow the exact control of the Au NPs size distribution when the Au loading is changed, therefore introducing too many variables that might be responsible for catalytic changes.[14,24] Common feature observed in TEM images for all hybrids of Au-**1**/TiO_2 A type is the placement of Au NPs, which, in spite of 2D nature of TEM images, often seems to be on the lateral surface of TiO_2 NPs. This was additionally confirmed by high angle annular dark-field scanning transmission electron microscopy (HAADF-STEM) images in which the brightness of the imaged samples is determined by atomic number and the thickness of the sample. As it can be seen in Figure 3a,b and Figure S3a,b (Supporting Information) both TEM and HAADF-STEM images indicate that Au NPs in type A hybrid are positioned on the lateral surface of the TiO_2 material. In contrast, such distribution of Au NPs is scarcely (and only in high loading Au hybrids) found in hybrids of the Au-**1**/TiO_2B. This difference can be explained by employed synthetic routes (Figure 2; see Supporting Information for further explanation). Namely, in Au-**1**/TiO_2A, prepared using linker coated Au NP, exposed catechol groups of the linker-**1** readily attach to the TiO_2 NPs forming a nanocomposite in which Au NPs can be observed attached to the surface of the TiO_2 (Figure 2a). On the other hand, when the AuNP-**1** seed-TiO_2 precursor methodology is used (type B composite), resulting Au-**1**/TiO_2B hybrid contains Au NPs embedded within the shell of TiO_2 crystalline material (Figure 2b), confirmed to be anatase by Raman spectroscopy (Supporting Information, Figures S9,S10).[25] Detailed TEM and HAADF-STEM (Supporting Information, Figures S4a,b) analysis also indicated uniform distribution of Au NPs within the TiO_2 matrix. Further confirmation of such arrangement of AuNPs-**1** came from the zeta potential measurements. As mentioned before, the zeta potential of AuNPs-**1** is –43 mV, while the potentials of commercial and synthesized TiO_2 (TiO_2NP A and TiO_2NP B respectively) are around –20 mV (all measured in phosphate buffer, pH = 6.0). When the zeta potentials of the type A hybrids were measured, a steady decrease from –33 mV for 0.1% to –38 mV for 50% Au loading was observed due to the increasing amount of Au NPs on the surface of the hybrids (Supporting Information, Figure S8a).

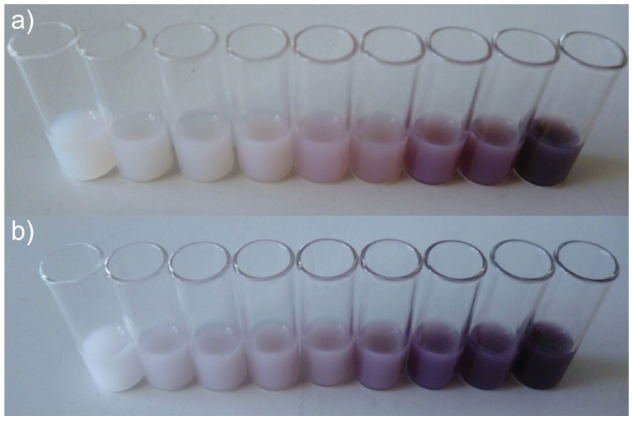

Figure 3. Colour changes observed in the suspension of a) Au-**1**/TiO_2A and b) Au-**1**/TiO_2B nanocomposite in pH 6 phosphate buffer with increasing wt% of Au (0.1, 0.25, 0.5, 1, 2, 5, 10, 20, and 50 from left to right hand side).

On the other hand, the increase in Au loading in type B hybrid does not change the surface properties of the hybrid itself as the particles are embedded in TiO_2 matrix and this is confirmed by the value of zeta potential which remains around ≈30 mV for all type B hybrids (with zeta potential of pure TiO_2B being around –30 mV) (Supporting Information, Figure S8b). When control samples were investigated containing citrate coated AuNP-**2**, resulting Au-**2**/TiO_2A hybrids lacked the coloration of the Au-**1** counterpart (data not shown), indicating that the bifunctional linker-**1** plays an important role in the preparation

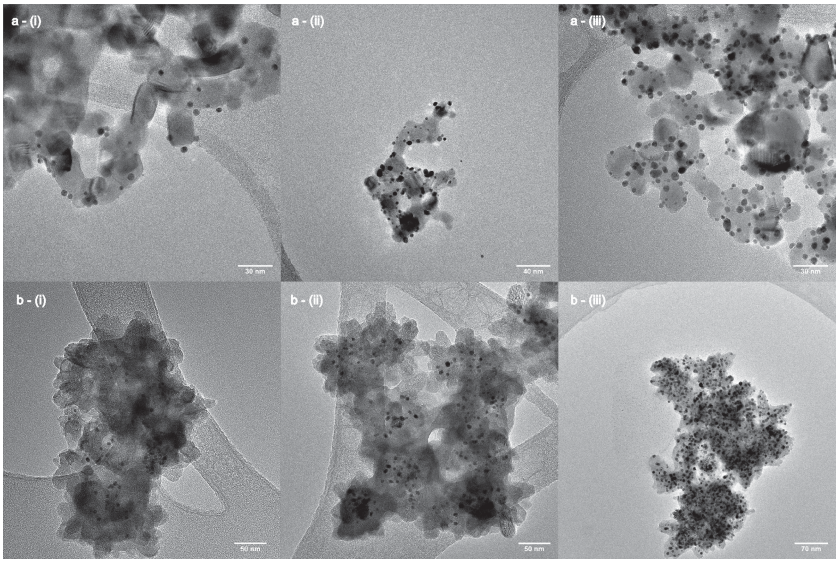

Figure 4. TEM images of a) Au-**1**/TiO_2A nanocomposite with i) 0.5 wt%, ii) 5 wt%, iii) 50 wt% of Au-**1** and b) Au-**1**/TiO_2B i) 0.5 wt%, ii) 5 wt%, and iii) 50 wt% Au-**1**.

of the Au/TiO_2 nanocomposites. TEM analysis of Au-**2**/TiO_2A hybrids showed that almost no Au NPs can be observed even for the higher Au loadings (Supporting Information, Figure S7a), confirming our assumption about the importance of linker-**1** for attachment of Au NPs to the TiO_2 surface. In the case of type B hybrid, AuNPs-**2** were found to be uniformly embedded within the TiO_2 material (Supporting Information, Figure 7b), indicating that the choice of the linker does not play an important role in the resulting distribution of Au NPs in type B hybrids.

2.2. Characterization of Hybrid Materials Using UV-Vis Spectroscopy

Further characterization of Au-**1**/TiO_2A and Au-**1**/TiO_2B hybrids was performed using UV-Vis absorption spectroscopy. Obtained spectra can be utilized for the study of the Au NPs plasmon band shift due to the presence of TiO_2 in their vicinity. Nanosized semiconducting TiO_2 has been already shown to have high absorption in the UV part of the spectrum (3.0–3.2 eV), which we confirmed from the measured absorption peaks around 340 nm in both hybrids.[26] As shown in **Figure 5**a,b, 550 and 580 nm Au NPs plasmon peaks are visible for Au-**1**/TiO_2A and Au-**1**/TiO_2B hybrid, respectively, AuNPs-**1** plasmon peek being at 519 nm (Supporting Information, Figure S1). Bigger red shift in the Au-1/TiO_2B hybrid indicates that there is a larger effect of TiO_2 on Au NPs, which is in favor of the previous hypothesis of Au NPs being embedded with TiO_2 matrix, resulting in the change of the surrounding dielectric constant and shift of the plasmon peak towards the longer wavelengths.

2.3. Photocatalytic Activity of Au/TiO_2 Hybrid Materials

As indicated in the introduction, TiO_2 nanostructured materials, in particular when doped with noble metals or quantum dots, show high photocatalytic activity and have been shown to aid the generation of ROS species such as hydroxyl and superoxide radical and hydrogen peroxide (H_2O_2). [3a,14,21,27], The mechanism of the ROS production when the hybrid is irradiated by 365nm light is described by:

(1) $AuTiO_2 + h\nu$ (365 nm)$\rightarrow$ $AuTiO_2$ ($e_{CB} + h_{VB}$) $\rightarrow$ Au (e_{CB}) TiO_2 (h_{VB})
(2) Au(e_{CB}) + $O_2 \rightarrow$ Au + $O_2^{-}\cdot$
(3) TiO_2 (h_{VB}) + $H_2O \rightarrow$ TiO_2 (h_{VB}) + $H^+ + OH^- \rightarrow TiO_2 + H^+ + OH\cdot$
(4) $H^+ + O_2^{-}\cdot \rightarrow HO_2\cdot$
(5) $HO_2\cdot + \rightarrow HO_2\cdot H_2O_2 + O_2$
(6) $O_2^{-}\cdot + 2H^+ + \rightarrow$ Au (e_{CB}) Au + H_2O_2

The mechanism of charge separation changes when less energetic light of 470 nm wavelength is used. Here, the Au NPs are photoexcited due to their plasmon resonance. Electron and holes are formed, and the electrons (hot electrons) are injected into the TiO_2 conductive band while the holes stay in the Au NPs.[9c,23b,28] The following reactions are the same as in the previous case. We have recently used activation of horseradish peroxidase (HRP) to study the activity of different TiO_2 nanostructures such as nanorods and nanoparticles and their applicability for enzymatic activation.[29] Iron containing catalytic center of the peroxidase enzymes is activated by hydrogen peroxide to catalyze the oxidation of different organic species.[30] We have therefore designed an assay to assess the photocatalytic activity of hybrid materials based on the HRP

Table 2. Comparison of calculated and ICP-MS measured Au/Ti ratios for Au-1/TiO_2A and Au-1/TiO_2B hybrids.

Hybrid Type	Method	Au [%]								
Au-**1**/TiO_2A	Theory	0.1	0.25	0.5	1	2	5	10	20	50
	Experiment (ICP-MS)	0.09	0.19	0.42	0.87	1.81	4.61	9.71	19.35	43.47
Au-**1**/TiO_2B	Theory	0.1	0.25	0.5	1	2	5	10	20	50
	Experiment (ICP-MS)	0.13	0.47	0.74	1.53	2.78	6.89	13.51	24.77	58.58

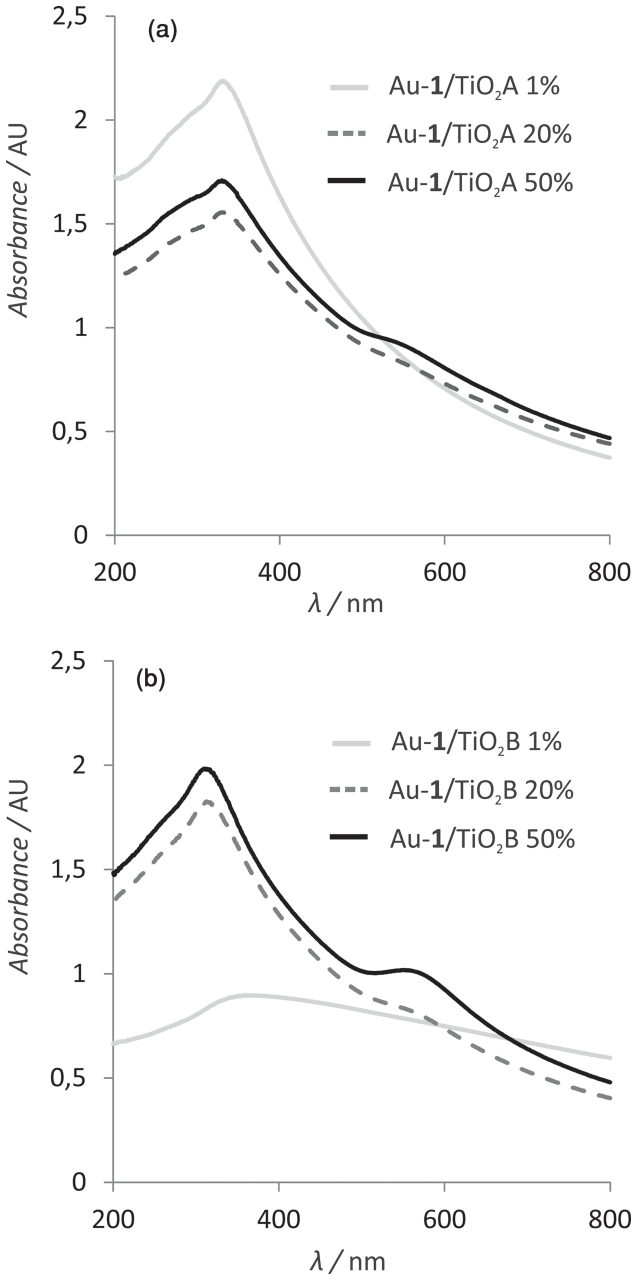

Figure 5. UV-Vis absorption spectra of a) Au-**1**/TiO_2A and b) Au-**1**/TiO_2B hybrids with different Au loadings (1, 20, and 50% Au)

activation and the subsequent oxidation of its substrate, ampliflu red (**Figure 6**). Non fluorescent Ampliflu red is oxidized into highly fluorescent product in the presence of HRP, which is activated by the ROS produced upon the irradiation of Au/TiO_2 hybrid material (controls were made to ensure that the ampliflu red does not oxidize only due to the presence of radicals, data not shown). Hence, on one hand, the photocatalytic activity is directly assessed by the fluorescence measurements (Figure 6) and, on the other hand, the efficiency of the hybrid system is studied on a biological platform paving a way for design of artificial catalytic systems based on enzymatic reactions.

2.3.1. Catalytic Activity Under Visible Light Irradiation

As it can be seen in **Figure 7**, Au-**1**/TiO_2A hybrid material showed approximately 2.5–5.5 (depending on the Au loading) time more photocatalytic activity compared to commercial TiO_2 NPs from which it was prepared. When Au-**1**/TiO_2B hybrid was examined and compared to the pure TiO_2 NPs synthesized from the TiF_4 precursor (TiO_2NP B), it showed an increase from 3.5–21 times (depending on the Au loading). When the hybrids of type A and B were directly compared, type A showed superior activity and it was up to six times more active than type B hybrid. The aforementioned experiments were all done upon 365 nm irradiation. This result can be attributed to the Au loading as well as the positioning of the AuNPs on the surface of the commercial TiO_2 NPs, which enables Au NPs to act as efficient electron storage system, shifting the apparent Fermi level of the composite to the more negative values making the catalytic system more reductive, therefore increasing the rate of ROS production.[10c] Photocatalytic behavior of type A hybrids are in good agreement with the findings by Bamwenda et al., where the highest activity was observed at gold loading of 1–2%. [22] As it can be seen in Figure 7 the photocatalytic activity does not change significantly after 2 wt% Au. Type B hybrid exhibits the highest activity at 5% loading from which it slowly decreases as Au percentage is increased. The inferior photocatalytic activity of type B hybrid compared to type A hybrid can be explained by their structural aspects. Namely, Au NPs embedded within TiO_2 structures can still store electrons, however their immediate interaction with water and oxygen molecules on the surface is prevented by the layer of TiO_2 matrix leading to the less ROS produced than in the case of type A hybrid. The presence of the hydrogen peroxide as the main ROS was confirmed by the experiment where the peroxide scavenging enzyme catalase was used. After the light irradiation, 2.5 μL (10 mg mL^{-1}) of catalase was added to the controls prior to HRP and Ampliflu red addition, after which the fluorescence was measured. The catalase containing controls showed no fluorescence while the catalase free ones were highly fluorescent indicating the high production of peroxide by the hybrids (Supporting Information, Figure S11) (Equations 1–6). When a control material containing Au citrate, Au-**2**/TiO_2 type A and B were investigated, slight activity increase (≈1.13 times on average) was observed in comparison with commercial TiO_2 NPs standard although it was significantly lower than the activity of Au-**1**/TiO_2A hybrids (Supporting Information, Figure S12). There was also no apparent correlation between the Au loading and the photocatalytic activity, as all the samples with an exemption of 5% Au-**2**/TiO_2A had photoactivity similar to TiO_2 NP standard. TEM analysis has already revealed that in comparison with Au-**1** type hybrids, not many Au NPs can be observed in the controls containing Au citrate confirming that the bridging linker-**1** plays a significant role in the preparation of highly active hybrid catalysts. On the other hand, when Au-**2**/TiO_2B was compared to Au-**1**/TiO_2B there was a similar pattern in photocatalytic activity due to the structural similarity (Supporting Information, Figure S13).

2.3.2. Catalytic Activity Under Visible Light Irradiation

As both Au-**1**/TiO_2A and Au-**1**/TiO_2B absorb in the visible part of the light spectrum, we wanted to explore the photoactivation

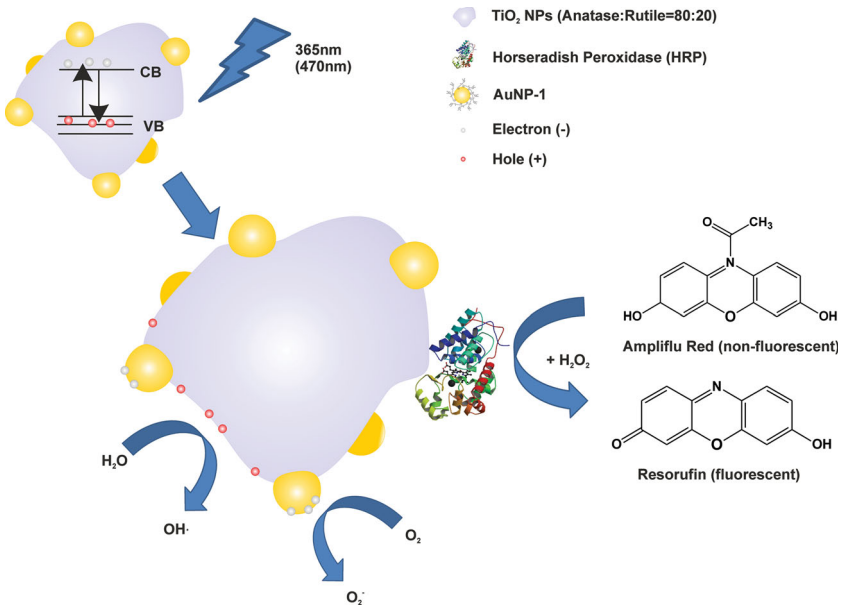

Figure 6. Photoexcitation of Au-**1**/TiO_2 hybrids and the principle of the enzyme activation and subsequent substrate oxidation, which can be assessed with fluorescence measurements.

and the catalytic performance of the systems when irradiated with visible light. Contrary to the results obtained with 365 nm irradiation, hybrids with lower content of Au do not show any significant difference in photocatalytic activity compared to standard TiO_2 NPs (commercial TiO_2NP A or synthesized TiO_2NP B). For both hybrid types, the activity steadily increases as the Au loading is increased (**Figure 8**), indicating that a different mechanism is involved, where the light energy is harvested by Au NPs followed by electron injection in the conduction band of adjacent TiO_2 NP or TiO_2 matrix as discussed earlier. In the case of hybrid type B, Au NPs are embedded in the reflective TiO_2 matrix, rendering them less accessible to visible light and therefore less ROS are produced. The difference in activity between the hybrids is ascribed to the presence of large amount of Au NPs on the surface of the TiO_2 NPs in type A, which can more readily absorb and scatter the incoming light.

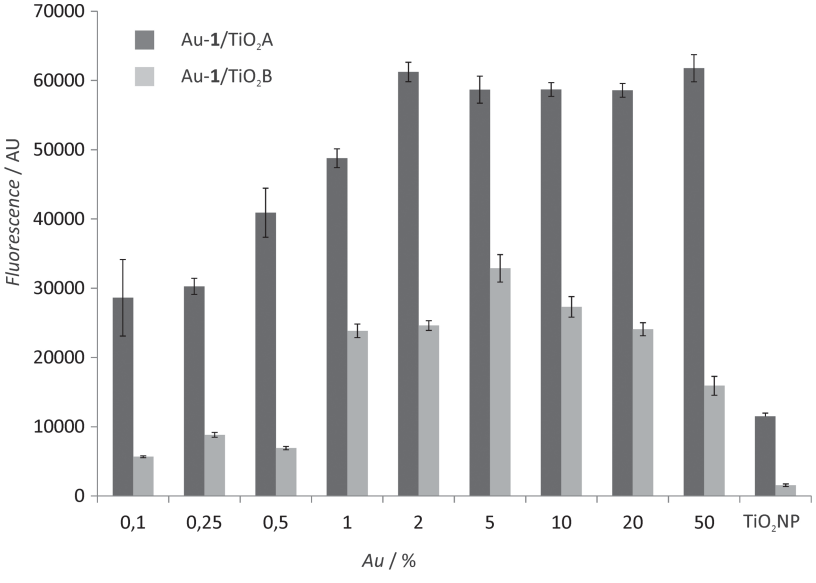

Figure 7. Photocatalytic activity/enzyme activation of Au-**1**/TiO_2A and Au-**1**/TiO_2B under 365 nm irradiation.

2.4. Switchability of the Enzymatic Activity in Presence of Au/TiO_2 Hybrid Materials

Finally, we were interested to see if we can achieve temporal control over the enzyme activation as demonstrated by Fruk et al. in case of ROS producing, photoactivatable CdS quantum dots.[30b] Herewith, we have prepared the solution of HRP, Ampliflu red and hybrid materials and irradiated it with two different light sources (365 and 470 nm) in regular intervals (2 min). It can clearly be seen from **Figure 9** that the oxidation of the Ampliflu red increases only when irradiated with UV (Figure 9a) or visible light (Figure 9b) (ON state) indicating that the enzyme is activated upon the irradiation of the hybrid material. The same is true for control TiO_2 NP although the photocatalytic activity is lower as seen from fluorescence intensities measured. When the light sources are switched off (OFF state) no activity increase can be observed. Results shown in Figure 9a are in excellent agreement with the 365 nm photocatalytic enzyme activation of the Au-**1**/TiO_2A hybrid made in the previous section. The increase of Au loading in the hybrids leads to the increase of fluorescence, which is in direct correlation with the enzyme activity. The 365 nm HRP photoswitchability is also possible with the Au-**1**/TiO_2B, however the resulting fluorescence is lower as it is in the ROS assay case (Supporting Information, Figure S14). In case of 470 nm irradiation (Figure 9b), the best results were obtained for 50% Au-**1**/TiO_2A and 50% Au-**1**/TiO_2B confirming the results obtained previously with standard enzymatic assay.

3. Conclusion

We have successfully prepared Au/TiO_2 nanocomposites using bifunctional, Au and TiO_2 binding linker, which showed significant increase in photocatalytic activity and activation of peroxidase enzyme compared to commercial TiO_2 NPs. The synthetic method is simple and allows a good control of both Au NPs size distribution and Au loading range (0.1 to 50%). Although UV light is often used to activate TiO_2 based catalysts, the presence of Au NPs enables the use of

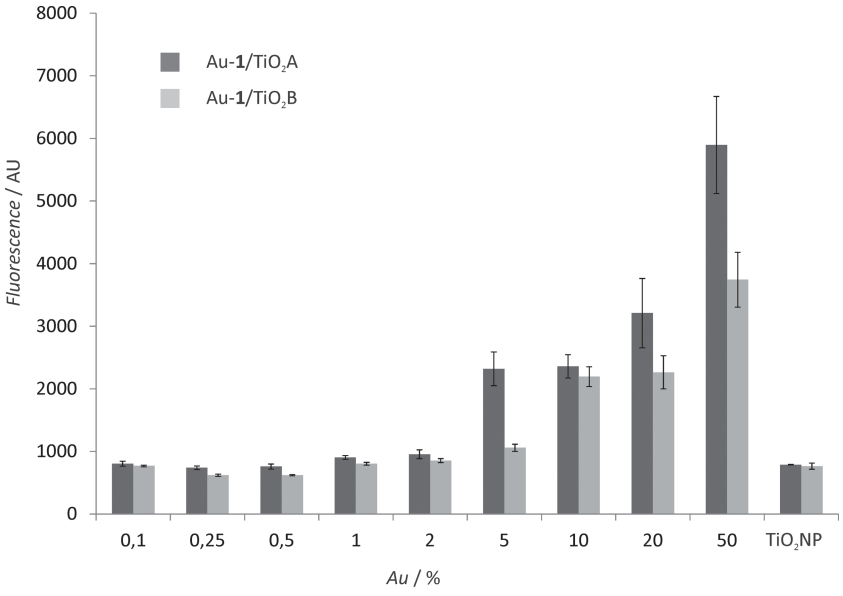

Figure 8. Photocatalytic activity of Au-**1**/TiO_2A and Au-**1**/TiO_2B when irradiated with visible light (470 nm) in presence of 1.33 μM HRP and 0.9 mM Ampliflu Red.

visible light (lower energy) for activation, which is of particular interest for biological applications. Contrary to previous reports we have observed that in some hybrids the higher content of Au NPs leads to the increase of the catalytic activity of prepared material when 365 nm light source is used. On the other hand, irradiation with visible light (470 nm) the photocatalytic activity of the hybrids increases with the Au loading. We believe that this type of material would find applications in catalysis, in particular light triggered enzyme activation or waste product removal and our efforts are currently focused on the use of reported and new bi-functional linkers to design hybrid materials with different metallic and oxide NPs for environmental applications.

4. Experimental Section

Materials and Methods: All chemicals were obtained from Sigma-Aldrich and used without further modification unless otherwise stated.

Synthesis of N-(3,4-dihydroxyphenethyl)-5-(1,2-dithiolan-3-yl) pentanamide (Lipoic Acid-Dopamine Linker) 1: Coupling of lipoic acid to dopamine hydrochloride was performed according to the literature procedure. [31]

Dicyclohexylcarbodiimide (1.00 eq) was added to a solution of dopamine hydrochloride (1.00 eq), DMAP (0.05 eq), and (*R*)-R-lipoic acid (1.00 eq) in dry pyridine. The reaction mixture was stirred for about 12 h at room temperature under anhydrous conditions. After evaporation under vacuum, the crude product was purified by column chromatography with CH_2Cl_2/CH_3OH 19:1.Yield: 30%; ^{1}H-NMR (250 MHz, $CDCl_3$, δ): 6.59–6.69 (m, 3 H, H_{Ar}), 3.50–3.61 (m, 3 H, CH and CH_2CO), 3.12–3.20 (m, 2 H, CH_2), 2.64 (t, ^3J = 7.2 Hz, 2 H, CH_2), 2.38–2.52 (m, 1 H, CH_2), 2.16 (t, ^3J = 7.2 Hz, 2 H, CH_2), 1.80–1.94 (m, 1 H, CH_2), 1.51–1.74 (m, 4 H, 2 × CH_2), 1.35–1.46 (m, 2 H, CH_2); MS (FAB, 3-NBA): *m/z* (%) = 107 (28), 225 (40), 342 (100) [M+H]+.

Preparation of Au/TiO_2 Hybrid: The synthesis of the hybrid Au/TiO_2 material was performed in two steps. First, Au NPs containing linker-**1** were prepared: aqueous solution of $HAuCl_4$ (50.8 mM) was mixed in Mili-Q water with EtOH solution of linker-**1**, the molar ratio n(Au^3+) to n(linker-**1**) being 10:1. The mixture was stirred for 1 h at RT, followed by the reduction of Au^{3+} by addition of $NaBH_4$ (10 mM) aliquots so that the end ratio of n(Au^{3+}) to n(BH_4^-) was 2:1. Resulting batch of AuNP-**1** was then, in the second step, used as a starting material for preparation of two different types of hybrids. Hybrid of type A, Au-**1**/TiO_2A, was prepared using commercially available TiO_2 NPs (P-25, Sigma) which were mixed with AuNP-**1** and refluxed for 1 h. Hybrid type B, Au-**1**/TiO_2B, was prepared using TiF_4 as a precursor and AuNP as seeds for the growth of TiO_2 shell. Appropriate amount of AuNP-**1** (Au ≈0.23 mg m^{-1}) were mixed with suspension (in Mili-Q water) of TiO_2NPs (1 mg mL^{-1}) to obtain Au loadings of 0.1, 0.25, 0.5, 1, 2, 5, 10, 20, and 50 wt%. The mixture was stirred vigorously and brought to boil for 1 h, after which it was cooled down, centrifuged and washed 3 times with Mili-Q water prior to further use. The synthesis of control hybrids using Au NPs stabilized with citrate linker-**2**[32] as starting material, was prepared as described above. All samples were weighed and dispersed in phosphate buffer (PB, pH = 6.0) in 1mg mL^{-1} concentration.

Material Characterization: UV-Vis spectra were recorded using Varian Cary-300 Spectrophotometer (Agilent). TEM images were obtained using a CM200-FEG microscope (Philips) operating at 200 kV together with selected area electron diffraction (SAED). Further TEM imaging, HAADF-STEM and energy dispersive X-ray spectroscopy (EDXS) were done on the *T*itan^3 80-300 TEM microscope (FEI) operating at 300 kV. Nano Zeta-Sizer (ZS Nano, Malvern) was used for DLS and zeta potential measurements. Fluorescence enzymatic assays were performed using Synergy H1 Hybrid Multi-Mode Micro-plate Reader (Biotek). ICP-OES and ICP-MS measurements were performed using OPTIMA 4300 DV from PerkinElmer and 7500ce from Agilent respectively.

ICP-MS, ICP-OES: Sample preparation: Every sample was shaken for 20 s. With a single channel pipette 100 μL up to 400 μL has been taken out of the sample holder into a 50 mL auto sampler vial. This has been repeated for every sample twice or three times. To dissolve the hybrid nanoparticles a mixture of 6 mL HCl sub-boiled, 2 mL HNO_3 sub-boiled and 1 mL HF Suprapur reagent (Merck Millipore) has been added to the samples. The chemical digestion has been carried out by 80 °C in a drying oven over night. Afterwards the acid solution has been diluted to 40 mL. Measurement: Both elements were determined by optical emission spectrometry (ICP-OES, OPTIMA 4300 DV from PerkinElmer). The dilution factor for Ti was 10 to 25 and for Au 10. The matrix solution was 5% nitrohydrochloric acid. The analysis was accomplished with four different calibration solutions and an internal standard (Sc). The range of the calibration solutions did not exceed one power of ten. The three major wavelengths have been used for calculation. Because of the better detection limit for Au most of the samples were analyzed with ICP-MS (Agilent 7500ce) as well. The dilution factor of the samples for Au was 5 to 50 in a matrix solution of 5 % nitrohydrochloric acid. Indium (In) has been used as an internal standard. The range of the calibration solutions did not exceed one power of ten. The mass 197 for Au and 115 for In has been used for the calculation of the results. The analysis has been repeated three times in a row. These implemented actions ensure an accurate determination of the titanium and gold content with less than 2% relative standard deviation and an error of measurement less than 3%.

TEM Imaging: TEM samples were prepared by putting droplets of sample suspension onto a 400 μm mesh copper TEM grid covered with a thin amorphous carbon film of less than 3 nm nominal thickness. Subsequently the prepared samples were dried in air at room temperature.

Study of Photocatalytic Activity: The photocatalytic activity was assessed using HRP–AR (Amplex red) assay. In a black 96 well-plate,

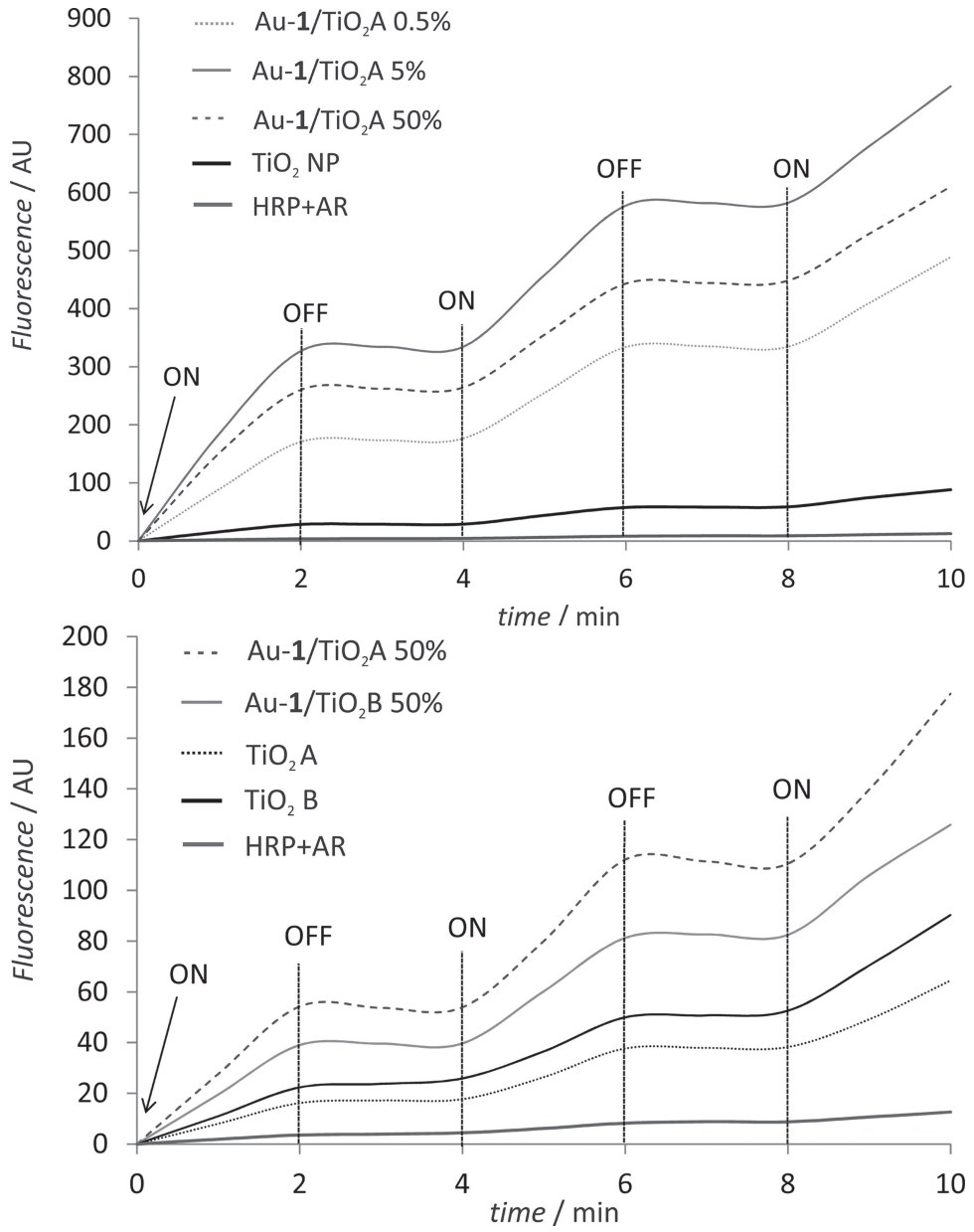

Figure 9. Photoswitchability of HRP by a) Au-**1**/TiO_2A hybrids using 365 nm light irradiation and b) most active 50% Au-**1**/TiO_2A and 50% Au-**1**/TiO_2B hybrids using 470 nm.

10 µL of sample (1mg mL^{-1}) was dispersed in phosphate buffer (PB, pH = 6.0) so that the total amount of liquid in the well prior to irradiation was 100 µL. The plates were then placed into custom made irradiation device where a row of LED diodes of wanted wavelength (366 nm or 470 nm) irradiated the plate wells for a period of 10min. 40 µL HRP (1.33 µM) and 10 µL AR (900 µM) were then added to irradiated wells, mixed 30 s and fluorescence measured using multi well plate reader. For the control experiments, either AR or HRP were not added. For the main ROS determination, 2.5 µL (10 mg mL^{-1}) of catalase was added prior to HRP and AR addition. The sensitivity of the instrument was set fixed to 65 and excitation and emission wavelengths were 540 and 585 nm respectively.

Light Controlled Activity of Horseradish Peroxidase: 10 µL (1 mg mL^{-1}) of hybrid were added to quartz cuvette containing 2 mL PB (pH = 6.0) followed by addition of 500 µL HRP (1.33 µM) and 200 µL AR (0.9 mM) and stirring. The cuvette was interchangeably kept in dark and irradiated by 366 nm UV hand lamp (4 W) (or 470 nm LED array) in periods of 2 min with fluorescence measurement every minute. The excitation and emission slits were set to size 5 and 2.5 respectively. The total duration of the experiment was 10 min.

Supporting Information

Supporting Information is available from the Wiley Online Library or from the author.

Acknowledgements

This work was supported by DFG-CFN Excellence Grant A5.7 and DAAD PhD studentship awarded to M.M. and partially carried out with support

of the Karlsruhe Nano Micro Facility (KNMF, www.knmf.kit.edu), a Helmholtz research infrastructure at Karlsruhe Institute of Technology (KIT, www.kit.edu).

Received: April 30, 2013
Published online: September 9, 2013

[1] a) X. Chen, S. S. Mao, *Chem. Rev.* **2007**, *107*, 2891–2959; b) S. W. Liu, J. G. Yu, M. Jaroniec, *J. Am. Chem. Soc.* **2010**, *132*, 11914–11916; c) X. J. Feng, K. Zhu, A. J. Frank, C. A. Grimes, T. E. Mallouk, *Angew. Chem. Int. Ed.* **2012**, *51*, 2727–2730.
[2] W. H. Leng, P. R. F. Barnes, M. Juozapavicius, B. C. O'Regan, J. R. Durrant, *J. Phys. Chem. Lett.* **2010**, *1*, 967–972.
[3] a) A. Fujishima, X. T. Zhang, *C. R. Chim.* **2006**, *9*, 750–760; b) L. Gomathi Devi, G. Krishnamurthy, *J. Phys. Chem. A* **2011**, *115*, 460–469.
[4] a) D. Lawless, N. Serpone, D. Meisel, *J. Phys. Chem.* **1991**, *95*, 5166–5170; b) K. Vinodgopal, P. V. Kamat, *Environ. Sci. Technol.* **1995**, *29*, 841–845.
[5] C.-T. Chen, J.-Q. Kao, C.-Y. Liu, L.-Y. Jiang, *Catal. Sci. Technol.* **2011**, *1*, 54–57.
[6] a) R. Dastjerdi, M. Montazer, *Colloids. Surf., B* **2010**, *79*, 5–18; b) R. Dastjerdi, M. Montazer, S. Shahsavan, *Colloids. Surf. B* **2010**, *81*, 32–41.
[7] G. Cernuto, N. Masciocchi, A. Cervellino, G. M. Colonna, A. Guagliardi, *J. Am. Chem. Soc.* **2011**, *133*, 3114–3119.
[8] J. Zhang, Q. Xu, Z. Feng, M. Li, C. Li, *Angew. Chem. Int. Ed.* **2008**, *47*, 1766–1769.
[9] a) S. D. Jhaveri, D. A. Lowy, E. E. Foos, A. W. Snow, M. G. Ancona, L. M. Tender, *Chem. Commun.* **2002**, 1544–1545; b) B. I. Ipe, K. G. Thomas, S. Barazzouk, S. Hotchandani, P. V. Kamat, *J. Phys. Chem. B* **2002**, *106*, 18–21; c) S. Mubeen, G. Hernandez-Sosa, D. Moses, J. Lee, M. Moskovits, *Nano Lett.* **2011**, *11*, 5548–5552.
[10] a) M. Jakob, H. Levanon, P. V. Kamat, *Nano. Lett.* **2003**, *3*, 353–358; b) A. Takai, P. V. Kamat, *ACS Nano* **2011**, *5*, 7369–7376; c) V. Subramanian, E. E. Wolf, P. V. Kamat, *J. Am. Chem. Soc.* **2004**, *126*, 4943–4950; d) P. D. Cozzoli, M. L. Curri, A. Agostiano, *Chem. Commun.* **2005**, 3186–3188.
[11] a) Y. Tian, T. Tatsuma, *J. Am. Chem. Soc.* **2005**, *127*, 7632–7637; b) A. Furube, L. Du, K. Hara, R. Katoh, M. Tachiya, *J. Am. Chem. Soc.* **2007**, *129*, 14852–14853.
[12] a) M. Valden, X. Lai, D. W. Goodman, *Science* **1998**, *281*, 1647–1650; b) X. F. Lai, D. W. Goodman, *J. Mol. Catal. A* **2000**, *162*, 33–50.
[13] E. Kowalska, R. Abe, B. Ohtani, *Chem. Commun.* **2009**, 241–243.
[14] A. Tanaka, A. Ogino, M. Iwaki, K. Hashimoto, A. Ohnuma, F. Amano, B. Ohtani, H. Kominami, *Langmuir* **2012**, *28*, 13105–13111.
[15] a) Z. W. Seh, S. Liu, M. Low, S. Y. Zhang, Z. Liu, A. Mlayah, M. Y. Han, *Adv. Mater.* **2012**, *24*, 2310–2314; b) Z. W. Seh, S. H. Liu, S. Y. Zhang, M. S. Bharathi, H. Ramanarayan, M. Low, K. W. Shah, Y. W. Zhang, M. Y. Han, *Angew. Chem. Int. Ed.* **2011**, *50*, 10140–10143.
[16] H. Yuzawa, T. Yoshida, H. Yoshida, *Appl. Catal. B* **2012**, *115*, 294–302.
[17] D. R. Pernik, K. Tvrdy, J. G. Radich, P. V. Kamat, *J. Phys. Chem. C* **2011**, *115*, 13511–13519.
[18] a) Z. Wang, X. W. Lou, *Adv. Mater.* **2012**, *24*, 4124–4129; b) A. Primo, A. Corma, H. Garcia, *Phys. Chem. Chem. Phys.* **2011**, *13*, 886–910.
[19] a) S. Swetha, S. M. Santhosh, R. G. Balakrishna, *Photochem. Photobiol.* **2010**, *86*, 628–632; b) M. N. Tahir, P. Theato, P. Oberle, G. Melnyk, S. Faiss, U. Kolb, A. Janshoff, M. Stepputat, W. Tremel, *Langmuir* **2006**, *22*, 5209–5212.
[20] V. Subramanian, E. E. Wolf, P. V. Kamat, *Langmuir* **2003**, *19*, 469–474.
[21] W. Li, J. P. Yang, Z. X. Wu, J. X. Wang, B. Li, S. S. Feng, Y. H. Deng, F. Zhang, D. Y. Zhao, *J. Am. Chem. Soc.* **2012**, *134*, 11864–11867.
[22] G. R. Bamwenda, S. Tsubota, T. Nakamura, M. Haruta, *J. Photochem. Photobiol. A* **1995**, *89*, 177–189.
[23] a) M. Murdoch, G. I. N. Waterhouse, M. A. Nadeem, J. B. Metson, M. A. Keane, R. F. Howe, J. Llorca, H. Idriss, *Nat. Chem.* **2011**, *3*, 489–492; b) C. G. Silva, R. Juarez, T. Marino, R. Molinari, H. Garcia, *J. Am. Chem. Soc.* **2011**, *133*, 595–602.
[24] A. A. Ismail, D. W. Bahnemann, I. Bannat, M. Wark, *J. Phys. Chem. C* **2009**, *113*, 7429–7435.
[25] a) C. J. Howard, T. M. Sabine, F. Dickson, *Acta. Crystallogr. B* **1991**, *47*, 462–468; b) H. X. Li, Z. F. Bian, J. Zhu, Y. N. Huo, H. Li, Y. F. Lu, *J. Am. Chem. Soc.* **2007**, *129*, 4538.
[26] a) K. M. Reddy, S. V. Manorama, A. R. Reddy, *Mater. Chem. Phys.* **2003**, *78*, 239–245; b) B. Geiseler, L. Fruk, *J. Mater. Chem.* **2012**, *22*, 735–741.
[27] G. S. Li, D. Q. Zhang, J. C. Yu, *Environ. Sci. Technol.* **2009**, *43*, 7079–7085.
[28] Z. Zhang, L. Zhang, M. N. Hedhili, H. Zhang, P. Wang, *Nano Lett.* **2013**, *13*, 14–20.
[29] B. Geiseler, M. Miljevic, P. Müller, L. Fruk, *J. Nanomater.* **2012**.
[30] a) E. Derat, S. Cohen, S. Shaik, A. Altun, W. Thiel, *J. Am. Chem. Soc.* **2005**, *127*, 13611–13621; b) L. Fruk, V. Rajendran, M. Spengler, C. M. Niemeyer, *ChemBioChem* **2007**, *8*, 2195–2198.
[31] A. Di Stefano, P. Sozio, A. Cocco, A. Iannitelli, E. Santucci, M. Costa, L. Pecci, C. Nasuti, F. Cantalamessa, F. Pinnen, *J. Med. Chem.* **2006**, *49*, 1486–1493.
[32] W. Haiss, N. T. Thanh, J. Aveyard, D. G. Fernig, *Anal. Chem.* **2007**, *79*, 4215–4221.